International Journal of Nanomedicine

Dovepress
open access to scientific and medical research

Open Access Full Text Article

ORIGINAL RESEARCH

TB@PLGA Nanoparticles for Photodynamic/Photothermal Combined Cancer Therapy with Single Near-Infrared Irradiation

Yue Yang[1,*]
Taya Tang[1,*]
Bo Liu[1]
Jijing Tian[1]
Haiyan Wu[1]
Zhongjie Liu[1]
Zhaoping Liu[2]
Lei Zhang[2]
Huihui Bao[2]
Tianlong Liu[1]

[1]Laboratory of Veterinary Pathology and Nanopathology, College of Veterinary Medicine, China Agricultural University, Beijing, People's Republic of China; [2]China National Center for Food Safety Risk Assessment, Beijing, People's Republic of China

*These authors contributed equally to this work

Background: Phototherapy has significant potential as an effective treatment for cancer. However, the application of a multifunctional nanoplatform for photodynamic therapy (PDT) and photothermal therapy (PTT) at a single excitation wavelength remains a challenge.

Materials and Methods: The double emulsion solvent evaporation method was used to prepare toluidine blue@poly lactic-co-glycolic acid (TB@PLGA) nanoparticles (NPs). The biocompatibility of TB@PLGA NPs was evaluated, and a 660 nm luminescence was used as the light source. The photothermal effect, photothermal stability, and singlet oxygen yield of NPs in an aqueous solution verified the feasibility of NPs as a PTT/PDT synergistic therapy drug.

Results: TB@PLGA NPs were successfully prepared and characterized. In vitro experiments demonstrated that TB@PLGA NPs can cause massive necrosis of tumor cells and induce apoptosis through a photodynamic mechanism under 660 nm laser irradiation. The TB@PLGA NPs also achieved optimal tumor inhibition effect in vivo.

Conclusion: The TB@PLGA NPs prepared in this study were applied as a dual-mode phototherapeutic agent under single laser irradiation. Both in vitro and in vivo experiments demonstrated the good potential of PTT/PDT for tumor inhibitors.

Keywords: toluidine blue, single irradiation, antitumor, 660 nm, phototherapy

Introduction

As new non-invasive tumor therapies, phototherapies such as photodynamic therapy (PDT) and photothermal therapy (PTT) have attracted attention, owing to their advantages of less trauma, high controllability, and good targeting.[1–3] In PDT, photosensitizers absorb light and transfer near-infrared (NIR) light energy to oxygen for producing reactive oxygen species that kill tumor cells.[4,5] In PTT, photothermal agents can absorb NIR light and generate hyperthermia, resulting in cancer cell damage. However, both these therapies have limitations, such as insufficient oxygen impediment (hypoxia) in the case of PDT and up-regulated expression of heat shock proteins in the case of PTT.[6,7] To overcome these obstacles, PDT and PTT should be incorporated into a single system.[8] Nevertheless, most therapeutic agents used for PDT and PTT need to be excited by lasers of different wavelengths because of mismatched absorbance,[9] leading to a longer therapeutic time and higher treatment cost. Moreover, the combination of different agents used for PDT and PTT in a single system may be limited by

Correspondence: Tianlong Liu
Laboratory of Veterinary Pathology and Nanopathology, College of Veterinary Medicine, China Agricultural University, No. 2 West Road Yuanmingyuan, Beijing, 100193, People's Republic of China
Tel/Fax +86 010 62732843
Email liutianlong@cau.edu.cn

Huihui Bao
China National Center for Food Safety Risk Assessment, No. 37, Guangqu Road, Chaoyang District, Beijing, 100022, People's Republic of China
Tel +86 010 52165564
Fax +86 010 52165561
Email baohuihui@cfsa.net.cn

Received: 18 February 2021
Accepted: 4 May 2021
Published: 16 July 2021

the dissociation of these different agents from each other during circulation, resulting in low therapy efficacy.[10]

Toluidine blue shows a strong absorption band in the range of 620–660 nm, which is located in the "phototherapy window" (600–900 nm), light can penetrate the tissues to a large extent in this window.[11,12] As a safe and effective cationic photosensitizer, TB can accumulate in negatively charged mitochondria after entering the organism.[13,14] It should be noted that TB is not only a photothermal agent but also a safe and effective photosensitizer. Its potential in photodynamic tumor therapy has been demonstrated by inducing phototoxicity of a variety of tumor cells in vitro,[15] but its application in tumor photothermotherapy has not been reported to date. To address the above-mentioned problems, we designed and synthesized TB@PLGA nanoparticles (NPs) with uniform morphology, good stability, and excellent performance. In this system, TB was used as a photothermal and photosensitive trigger. In addition, the as-prepared TB@PLGA NPs had PDT and PTT functions under single wavelength laser irradiation to facilitate treatment efficiency.

In the present study, the PLGA NPs were prepared as described in a previous study.[16] The biocompatibility of TB@PLGA NPs was evaluated, and 660 nm luminescence was used as the light source. The photothermal effect, photothermal stability, and singlet oxygen yield of NPs in an aqueous solution verified the feasibility of NPs as a PTT/PDT synergistic therapy drug.

Materials and Methods

Materials

Toluidine blue, PLGA and PVA were purchased from Sigma Aldrich (Saint Louis, USA). Sodium chloride, ethyl acetate (EtAc) and Ethylene Diamine Tetraacetic Acid (EDTA) were purchased from Sinopharm Chemical Reagent Co., Ltd (Beijing, China). Dulbecco's modified eagle medium (DMEM), fetal bovine serum (FBS) and trypsin were purchased from Thermo Fisher Scientific (Waltham, USA). Annexin V-FITC kit was purchased from Beyotime Biotechnology Co., Ltd (Beijing, China).

Preparation of TB@PLGA Nanoparticles

A proper calculated amount of TB powder was dissolved in 3% NaCl to prepare 10 mg/mL TB solution as the internal water phase (W1). Then, 1 and 0.5% PVA solutions were used as the outer water phase (W2) and diffusion phase, respectively. To prepare the nanoparticles, PLGA (200 mg) was dissolved in different volumes of EtAc organic solvent (in different water oil ratios). After ultrasonic dispersion, PLGA was used as the oil phase (O). An appropriate amount of the internal water phase was slowly dropped into the oil phase, ultrasonicated for 8 min under ice bath condition (working for 2.5 s, pause for 2.5 s) to form the first emulsion. The prepared emulsion was slowly added to 10 mL of 1% PVA aqueous phase, and then ultrasonicated for 15 min under ice bath condition (working for 3 s, pause for 3 s) to obtain multiple emulsions. After stirring for 3–4 h, the oil phase was volatilized.

Characterization of TB@PLGA Nanoparticles

The Zetasizer nanoparticle size potentiometers (Zetasizer Nano ZS90; Malvern, UK) were used to determine the properties of TB@PLGA. The hydrodynamic particle size and electric potential of NPs were evaluated. The morphological characteristics of TB@PLGA NPs were observed by scanning electron microscopy (SEM, FEI Inspect F50, USA). The chemical structure of the TB@PLGA NPs was analyzed at the molecular level by Fourier transform infrared spectroscopy. The encapsulation efficiency and drug loading were measured by UV-Vis spectra.

Cell Culture

Intestinal epithelial cell line 6 (IEC-6), human hepatoma cells (Huh7) and breast cancer cells (4T1) were purchased from Shanghai Gaining Biological Technology Co. Ltd (Shanghai, China). Cell culture medium was DMEM or RPMI, 10% FBS and antibiotics. An incubator with 5% CO_2 was used to culture cells at 37 °C.

In vitro Toxicity

In vitro cell experiments and hemolysis tests were carried out to evaluate the safety of TB@PLGA NPs. IEC-6 cells were used to detect TB and TB@PLGA using the Cell Counting Kit-8 (CCK-8). Different concentrations were set for the dark toxicity (0.0625, 0.125, 0.25, 0.5, 1, 2, 4, and 8 μg/mL) with six parallel in each group.

According to the standard method, the normal saline group was used as the nonhemolytic negative control, and the 1% Triton X-100 group was used as the positive control of complete hemolysis. The final concentrations of TB@PLGA NPs were 10, 25, 50, 100 and 200 μg/mL.

Acute Toxicity Test in vivo

The BALB/c mice purchased from Beijing Vital River Laboratory Technology Co, Ltd. (Beijing, China) were randomly divided into four groups with four mice in each group with different doses (25, 75, 125 mg/kg). The mice were fed and managed by their tail vein, and the behaviors of veins, their feeding and drinking water behaviors were closely observed, and the death situations were counted. After 96 h, the mice were weighed, their eyeballs were excised to collect blood, and the mice were sacrificed after blood collection. Animal experimentation was governed by the Regulations for Experimental Animals of Beijing Authority. Animal Ethics Committee of the China Agriculture University approved the experiment.

Aqueous solutions of TB@PLGA NPs having different concentrations (5,10,15, 20 and 25 mg/mL) were prepared with deionized water. The temperature changes of the solutions upon irradiation of a 660 nm NIR laser (power density of 1 W/cm^2) were recorded using an FLIR imaging instrument. Deionized water acted as the control group. The photothermal stability of the solutions was also measured.

Photodynamic Effects in vitro

The singlet oxygen production capacities of TB and TB@PLGA NPs were measured by the chemical capture method under irradiation using a 660 nm NIR laser (the power density of 1 W/cm^2).

In vitro Antitumor Study

Different concentrations (100 and 200 μg/mL) of TB@PLGA NPs were cultured with Huh7 cells for 24 h. The cells in the light group were irradiated with a 660 nm laser for 5 min and then incubated for 30 min. Subsequently, all were stained with fluorescence. After incubating for 20 min at room temperature, the cells were observed using a fluorescence microscope.

In vivo Antitumor Study

BALB/c female mice were used to establish the mouse breast cancer model. In the antitumor activity study, 0.2 mL (1×10^8 cells/mL) of the 4T1 cells suspension was inoculated subcutaneously in the right armpit of mice. When the tumor volume was about 80 mm^3, the tumor bearing mice were randomly divided into six groups, with five mice in each group as follows: control group (5% glucose solution), 5% glucose solution + laser group, TB group, TB + laser groupTB@PLGA NP group, TB@PLGA NPs + laser group. The drug was administered by tail vein injection, The concentration of TB@PLGA NPs was 15 mg/mL, and that of TB group was 0.3 mg/mL. After 24 hours of administration, the mice of laser groups were anesthetized and then irradiated with laser (660 nm, 0.5 w/cm^2) for 5 min. The temperature changes of tumor were recorded by optical fiber probe. After treatment, the behaviors of mice were observed every day. The tumor volumes were measured every other day, and the curve of relative volume of tumor was drawn. After 16 days, the tumor was removed and photographed.

Statistical Analysis

The data were presented as means ± standard deviation (SD) and $p < 0.05$ was defined a statistically significant difference.

Results and Discussion

Toluidine blue play s a profound role in the field of medicine. It can be used as a nucleic acid dye for the detection of tumors in a clinic setting,[17,18] and as a safe and effective photosensitive material for both PDT and PTT.[19] However, it is aggregates easily at high concentrations, and the generation of polymers affects the photosensitivity. PLGA is an ideal carrier because of its stability, low toxicity, controllable biodegradation and good biocompatibility.[20] Therefore, the double emulsion solvent evaporation method[21] was used to prepare TB@PLGA NPs (Figure S1) to prevent the aggregation of TB. Different volume ratios of the TB and PLGA solutions were investigated to optimize the preparation conditions. As shown in Figure S2, the different solution ratios led to the formation of NPs with different particle sizes. The TB: PLGA volume ratio of 1:11, led to the formation of NPs with an average particle size 230 nm, which was ideal for our experiments.

The nanoparticle size is shown in Figure S3 shows that the average NP size was 232.6 nm and the polydispersity index (PDI) was 0.045. There was a negative charge on the surface of NPs, and the potential value was determined to be −18 ± 4.02 mV (Figure S4). As shown in Figure S5 and Figure 1A, at an accelerating voltage of 12.0 kV, the distribution was uniform, round and spherical. Moreover, the size was uniform (200 nm) and the surface of the spherical NPs was smooth, which is consistent with the results of Zetasizer nanoparticle size potentiometry. The morphology of NPs showed no significant change after seven days (Figure S6).

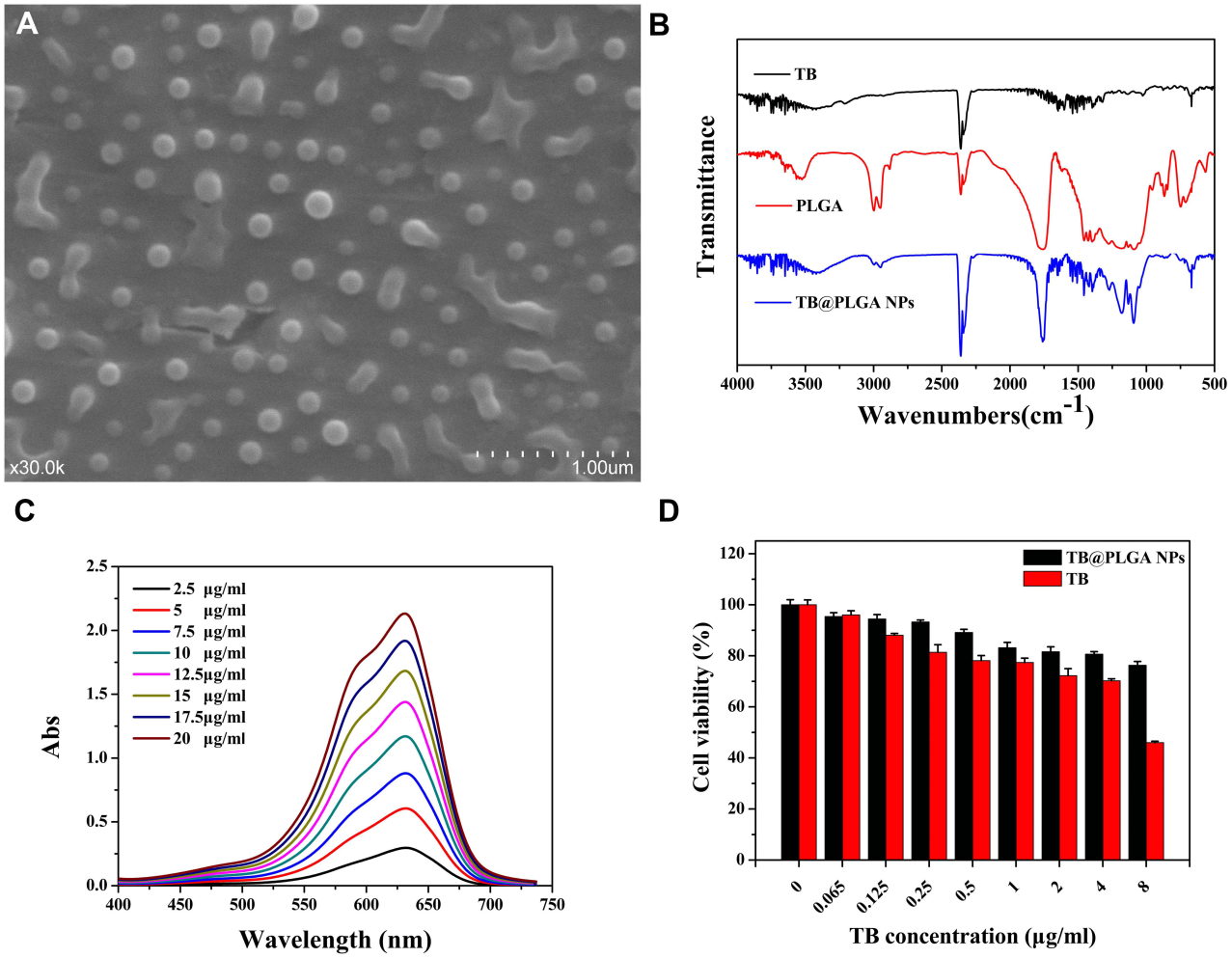

Figure 1 Characterization of TB@PLGA NPs. (**A**) SEM image (**B**) FTIR spectrum (**C**) UV absorption spectra (**D**) cell viability.

The results of Fourier transform infrared spectroscopy (FTIR) analysis of TB, PLGA and TB@PLGA are shown in Figure 1B. According to the structural formula of TB and PLGA, the peak at 669 cm^{-1} in their spectra can be attributed to the out-of-plane bending vibrations of the C-H homophase of the aromatic ring. The peaks at 1460 and 1373 cm^{-1} are caused by the in-plane C-H bending vibrations.In addition, the peak at 1600 cm^{-1} corresponded to the skeleton vibration of the benzene ring in the polymer, and the absorption peak at 3687 cm^{-1} was attributed to the N-H stretching vibrations. These results indicate that the NPs contained TB, PLGA, and TB@PLGA. In the FTIR spectrum of the NPs, the peak at 1384 cm^{-1} belonged to the stretching vibration of -CH3, while the peak at 1456 cm^{-1} was the characteristic of CH_2.The peak at 1756 cm^{-1} was attributed to the C=O stretching vibration, and the broad peak extending from 3400 to 3600 cm^{-1} was corresponded to the weak vibrations of end-OH moieties of the polymer. This indicated that PLGA was also present in the NPs. In other words, TB was successfully packaged into PLGA NPs.

As shown in Figure 1C, the maximum absorption peak of TB was located at 630 nm, and it had a strong absorption band in the range of 550–670 nm, which lies within the phototherapy window. This indicates that TB has good phototherapeutic potential. For this reason, a standard curve was drawn by linear regression analysis with TB concentration C (μg/mL) as the abscissa and TB solution absorbance at 630 nm as the ordinate. As shown in Figure S7, the linear regression equation y = 0.1052x + 0.0821 was obtained, with R^2 = 0.9969, which indicates a good linear relationship. The total volume of the supernatant solution obtained in the processing of NPs was measured. The ultraviolet absorbance of the supernatant was determined. The data was substituted into the regression equation of TB standard curve, and the concentration of TB in the supernatant was calculated. The entrapment efficiency

(EE) and drug loading (DL) of TB@PLGA NPs were were calculated to be 85.06% and 2.08%, respectively.

The cell viability results are shown in Figure 1D. With an increase in the concentration of TB@PLGA NPs and free TB, the cell activity decreased gradually, however, at the same concentration, the inhibition ratio of free TB related to the cell activity was higher than that of TB@PLGA NPs. When the effective concentration of TB was 8 μg/mL, the relative activity of cells was only 45% in the free TB group and 76% in the NP group. In the low concentration groups, when the effective concentration of TB was below 4 μg/mL, the relative activity of cells in the NP group was more than 80%. These results indicate that PLGA NPs have good biocompatibility as drug carrier materials. Compared with free TB, the toxic effect of TB@PLGA NPs on normal tissue cells was low. To assess the effect of photothermal heating of TB@PLGA NPs, a 660 nm (1 W/cm^2) laser was used to irradiate the material, and the temperature change was recorded using a thermal imager. As shown in Figure S8, the positive control Triton-X 100 group was completely hemolytic compared to the negative control group, and there was no obvious hemolysis in the experimental group. According to the measured absorbance of the supernatant, the hemolysis rate of red blood cells in the test group was lower than 5% at the five concentrations. When the concentration of TB@PLGA NPs was 200 μg/mL (highest concentration), the relative hemolysis rate was only 3.9%. At the same time, as seen under the microscope, red blood cells in the Triton-X 100 group were completely lysed, and some red blood cells had shrunk in the 200 μg/mL group. However, no abnormal red blood cells were found in the negative control group and other low concentration groups. Therefore, TB@PLGA NPs meet the requirements of hemolysis testing for clinical application of biomaterials specified by ISO and have good hemolytic safety.

The serum biochemical indexes of mice are shown in Table S1. At the concentrations of 25, 75 and 125 mg/kg, the three detection indexes of alanine aminotransferase (ALT), aspartate aminotransferase (AST), and urea nitrogen (BUN) were within the normal range. Moreover, there was no significant increase or decrease compared with the control group ($p>0.05$). As shown in Figure S9, the routine blood test results of each group were within the normal range. There were no significant differences in RBC, WBC, HGB, MCH, HCT and MCV as well as in the biological statistics between the control and the experimental groups ($p > 0.05$). This shows that TB@PLGA NPs do not cause abnormal changes in the blood properties of animals, which can otherwise result in a series of pathological reactions. As shown in Figure S10, the visceral body ratio of the mouse heart slightly increased in the three experimental groups, and the visceral body ratio of the spleen slightly increased in the low and medium dose groups, however, the visceral body ratio of the lung slightly decreased in the medium- and high-dose groups. In general, there was no significant difference in the organ coefficients between the two groups ($P > 0.05$). Thus, there was no abnormal effect of TB@PLGA NPs on the organs of mice.

Furthermore, there were no distinct ocular pathological changes in the main organs and tissues of the mice in each group after autopsy. The pathological sections are shown in Figure S11. No distinct abnormal lesions were found in the heart, liver, spleen, lung, kidney, and brain tissue sections of the four groups. There were no significant difference between the experimental group and the control group from low to high doses.

As shown in Figure 2A and B), within 10 min of illumination, the temperature rise amplitude of the control group (distilled water) was limited. After irradiation, the temperature of the TB@PLGA NPs solution increased to 49.2 °C in 5 mins, and to 53 °C in 10 min. Moreover, the temperature increased rapidly in the early stage and tended to increase gradually in the later stage. In addition, the heating effect of the TB@PLGA NPs exhibited a certain concentration dependence. When the concentration of NPs was more than 15 mg/mL, there was no significant difference in the temperature rise between the different concentration groups.Therefore, the concentration of TB@PLGA NPs was determined to be 15 mg/mL in the follow-up test. The photothermal stability of the TB@PLGA NPs was recorded via four cycles of laser irradiation. The results of the temperature rise of NPs were shown in Figure 2C. The rising trend of the sample temperature in each cycle was consistent, and the temperature peak value did not decrease, which indicated that TB@PLGA NPs have good photothermal stability.

The curve of the characteristic peak intensity of ultraviolet absorption of DPBF in TB and TB@PLGA NPs solutions with time was shown in Figure 2D and E. Based on this curve, samples were taken at six time intervals, and TB and TB@PLGA were drawn with time as abscissa and the decrease in the absorbance at the DPBF characteristic peak was the ordinate. The linear fitting curve of the singlet oxygen

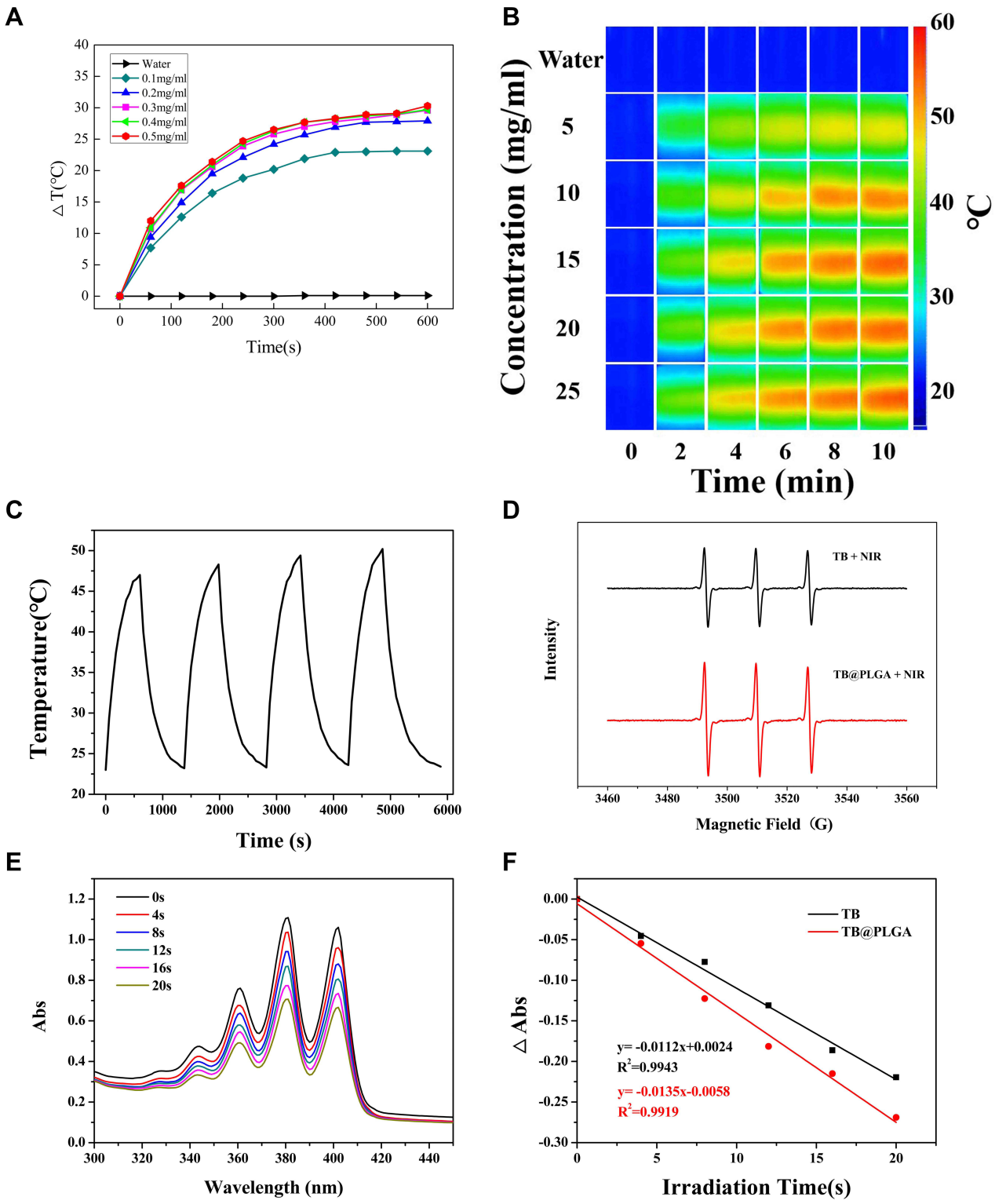

Figure 2 In vitro microwave heating properties. (**A** and **B**) Photothermal heating of TB @ PLGA NPs. (**C**) Photothermal stability of TB @ PLGA NPs. (**D**) ESR (**E**) Curves of DPBF UV absorption characteristic peak intensity change. (**F**) Linear fitting curve of singlet oxygen generation rate of TB and TB@ PLGA NPs.

generation rate of NPs was shown in Figure 2F. The absorbance at the characteristic absorption peak of DPBF showed a good linear relationship with irradiation time ($R1^2 = 0.9943$; $R2^2 = 0.9919$), and the slope k value was used as an index to evaluate the singlet oxygen production capacity. The slopes of TB and TB@PLGA NPs were 0.0112 and 0.0135,

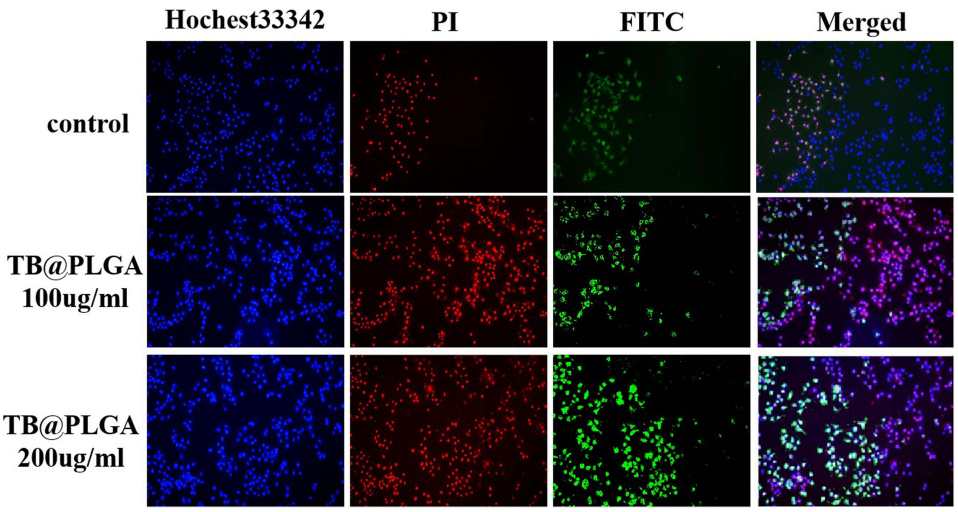

Figure 3 Fluorescence image of Huh7 cells after 660nm (1W) laser irradiation for 5min (10×).

respectively, which indicated that TB@PLGA NPs have a relatively strong tendency to produce singlet oxygen.

To evaluate the efficacy of TB@PLGA NPs as phototherapeutic agents, Hoechst 33342 and Annexin-V-FITC/PI double staining were used to detect the dead and living cells. The results were shown in Figure 3. The living cells are stained blue, early apoptotic cells are stained green, advanced apoptotic cells are stained both green and red, while necrotic cells are stained red. After laser irradiation, no apoptosis was observed in Huh7 cells treated with TB@PLGA NPs. When the concentration of NPs increased, the necrosis rate of Huh7 cells increased. Moreover, after the irradiation of Huh7 cells with a 660 nm laser (1 W/cm^2) for 5 min, the nuclei of the cells in each group showed a strong red fluorescence signal. Compared to the blank control group, the necrosis rate of tumor cells in the treated group was very high, and the number of apoptotic cells also increased. It can be preliminarily concluded that TB@PLGA NPs can cause physical and chemical damage to tumor cells through the photothermal effect, resulting in cell necrosis and apoptosis through a photodynamic mechanism.

As shown in Figure 4A and B, the temperature of the tumor site of TB@PLGA NPs group was significantly higher than those of the control and TB groups under the same light conditions. After illumination for 5 min, the temperature reached approximately 52 °C and the temperature rise was 22 °C. The warming trends of TB and TB@PLGA NPs were similar. In the early stage of irradiation, the temperature of the tumor reached 41°C after 2 min, subsequently, the heating rate slowed down and gradually reached a plateau. This result showed that TB@PLGA NPs accumulate in the tumor and produce an effective heat killing effect.

After laser treatment, there was no death in each group. According to the curve of relative tumor volume in Figure 4C and D, there was no significant difference in the tumor growth curve between the 5% glucose solution group and the 5% glucose solution + laser group. On the 16th day after treatment, the tumor volume of the two groups was 7.5 times the initial tumor volume. The results showed that laser irradiation alone had no distinct effect on tumor inhibition. The tumor growth curve of the TB group was similar to that of the control group, and the tumor growth volume was 6.9 and 7.2 times, respectively, which indicated that the TB had no dark toxicity and could not effectively inhibit the growth of the tumor. Compared with the control group, the TB + laser group had effects of reducing the tumor growth rate, but the tumor could not be completely eliminated. In the TB@PLGA NPs + laser group, the tumor was gradually ablated and the volume became smaller, eventually, the tumors of two mice in the group were completely ablated.

As shown in Figure S12, the 5% glucose solution group showed a normal histological state under both light and non-light conditions. Tumor cells were arranged closely, with large volume, deep staining of the nucleus, enlarged nucleolus, visible pathological mitosis, and no evident cell necrosis. Under no light conditions, in the TB and TB@PLGA NPs groups, the tumor cells were in disordered, with distinct heteromorphism, uneven distribution of chromatin, and different sizes and shapes of the nuclei, however, no evident damage was seen. Under light

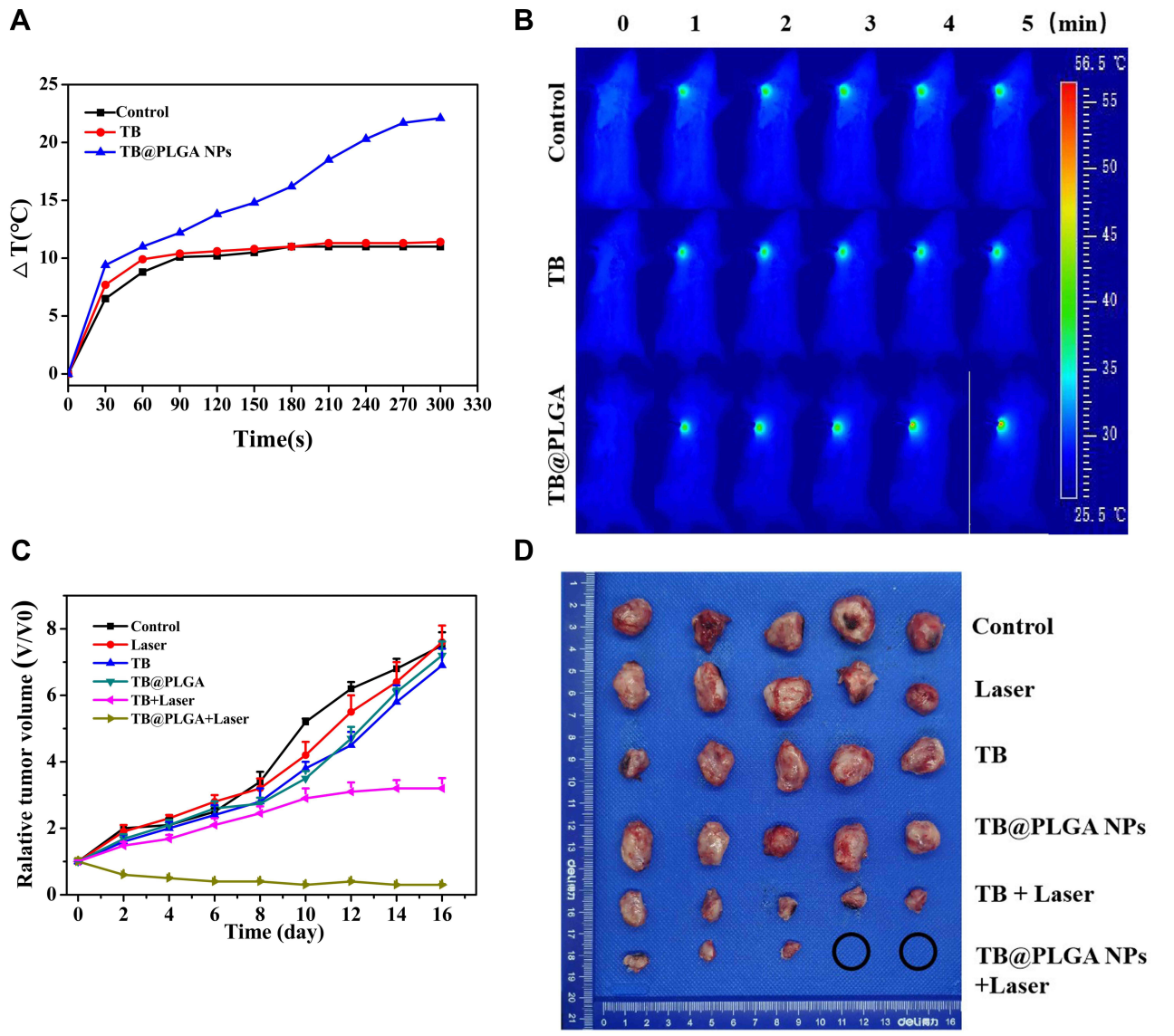

Figure 4 In vivo antitumor effects. (**A**) The temperature curves and (**B**) in vivo tumor thermal imaging of each group under light conditions. (**C**) Relative volume curves and (**D**) in vitro tumor images of mice tumors.

conditions, tumor cells in the TB group exhibited distinct cell necrosis, unclear cell boundaries in some areas, loose tumor tissue arrangement, cell rupture, and increased mitotic phase. The necrosis of tumor cells was more evident in the TB@PLGA NPs group, and a large area of tissue necrosis, nuclear condensation, rupture, dissolution, and multiple bleeding were observed in the ablation area.

Conclusion

In the present study, TB@PLGA NPs were successfully prepared. In the experimental dose range, the dark toxicity of these NPs toward tumor cells in vitro was very low, and no distinct stimulation effect was found in mice. Under 660 nm laser irradiation, the nanomaterials caused massive necrosis of tumor cells in vitro and induced apoptosis through a photodynamic mechanism. These nanomaterials were effective PTT and PDT agent at the tumor site simultaneously, achieving the ideal tumor inhibition effect in vivo; thus, they demonstrated the significant potential for the PTT/PDT of tumors.

Acknowledgments

The authors acknowledge financial support from Young Teachers Innovation Project of China Agricultural University (2018QC142). National Natural Science Foundation of China (Project No. 31802237) and Research and Development

Projects in Key Areas of Guangdong (2019B020210002). Yue Yang and Taya Tang are co-first authors for this study.

Disclosure

The authors report no conflicts of interest in this work.

References

1. Fantini S, Sassaroli A. Near-infrared optical mammography for breast cancer detection with intrinsic contrast. *Ann Biomed Eng*. 2012;40(2):398–407. doi:10.1007/s10439-011-0404-4
2. Chen M, Lin Z, Ling MH. Near-infrared light-activatable microneedle system for treating superficial tumors by combination of chemotherapy and photothermal therapy. *Acs Nano*. 2016;10(1):93–101. doi:10.1021/acsnano.5b05043
3. Zhao L, Yuan W, Tham HP, et al. Fast-clearable nanocarriers conducting chemo/photothermal combination therapy to inhibit recurrence of malignant tumors. *Small*. 2017;13:170096329. doi:10.1002/smll.201700963
4. Park D, Kim J, Choi Y. Photosensitizer-complexed polypyrrole nanoparticles for activatable fluorescence imaging and photodynamic therapy. *J Mater Chem B*. 2016;4(47):7545–7548. doi:10.1039/C6TB02461K
5. Chilakamarthi U, Giribabu L. Photodynamic therapy: past, present and future. *Chem Rec*. 2017;17(8):775–802. doi:10.1002/tcr.201600121
6. Shen Y, Huang M, You W, Luo X, Ke C. The survival and respiration response of two abalones under short-term hypoxia challenges. *Aquaculture*. 2020;529:735658. doi:10.1016/j.aquaculture.2020.735658
7. Lellahi SM, Rosenlund IA, Hedberg A, et al. The long noncoding RNA NEAT1 and nuclear paraspeckles are up-regulated by the transcription factor HSF1 in the heat shock response. *J Biol Chem*. 2018;293(49):18965–18976. doi:10.1074/jbc.RA118.004473
8. Liang P, Tang H, Gu R, et al. A pH-responsive zinc (II) metalated porphyrin for enhanced photodynamic/photothermal combined cancer therapy. *Sci China Mater*. 2019;62(8):1199–1209. doi:10.1007/s40843-019-9423-5
9. Sun P, Wang X, Wang G, et al. A perylene diimide zwitterionic polymer for photoacoustic imaging guided photothermal/photodynamic synergistic therapy with single near-infrared irradiation. *J Mater Chem B*. 2018;6(20):3395–3403. doi:10.1039/C8TB00845K
10. Zhao Z, Shi S, Huang Y, Tang S, Chen X. Simultaneous photodynamic and photothermal therapy using photosensitizer-functionalized Pd nanosheets by single continuous wave laser. *Acs Appl Mater Inter*. 2014;6(11):8878–8885. doi:10.1021/am501608c
11. Cancela-Rodriguez P, Cerero-Lapiedra R, Esparza-Gomez G, Llamas-Martinez S, Warnakulasuriya S. The use of toluidine blue in the detection of pre-malignant and malignant oral lesions. *J Oral Pathol Med*. 2011;40(4):300–304. doi:10.1111/j.1600-0714.2010.00985.x
12. Wainwright M, Giddens RM. Phenothiazinium photosensitisers: choices in synthesis and application. *Dyes Pigments*. 2003;57(3):245–257. doi:10.1016/S0143-7208(03)00021-4
13. Harris F, Sayed Z, Hussain S, Phoenix DA. An investigation into the potential of phenothiazinium-based photo-sensitisers to act as PDT agents. *Photodiagn Photodyn*. 2004;1(3):231–239. doi:10.1016/S1572-1000(04)00046-8
14. Wang X, Lei Q, Zhu J, et al. Cucurbit[8]uril regulated activatable supramolecular photosensitizer for targeted cancer imaging and photodynamic therapy. *Acs Appl Mater Inter*. 2016;8(35):22892–22899. doi:10.1021/acsami.6b07507
15. Graciano TB, Coutinho TS, Cressoni CB, et al. Using chitosan gels as a toluidine blue O delivery system for photodynamic therapy of buccal cancer: in vitro and in vivo studies. *Photodiagn Photodyn*. 2015;12(1):98–107. doi:10.1016/j.pdpdt.2014.11.003
16. Arafa MG, Mousa HA, Afifi NN. Preparation of PLGA-chitosan based nanocarriers for enhancing antibacterial effect of ciprofloxacin in root canal infection. *Drug Deliv*. 2020;27(1):26–39. doi:10.1080/10717544.2019.1701140
17. Nabeya D, Kinjo T, Yamaniha K, et al. Use of steroids to treat anti-tumor necrosis factor alpha induced tuberculosis-associated immune reconstitution inflammatory syndrome case report and literature review. *Medicine*. 2020;99(43):e22076. doi:10.1097/MD.0000000000022076
18. Yang J, Vuong K, Moodley A, et al. An unusual case of TB-associated acute demyelinating encephalomyelitis in a 7-month-old infant. *Neurology*. 2020;94S(15).
19. Zhang W, Tung C. Real-time visualization of lysosome destruction using a photosensitive toluidine blue nanogel. *Chem Eur J*. 2018;24(9):2089–2093. doi:10.1002/chem.201705697
20. De Negri Atanasio G, Ferrari PF, Campardelli R, et al. Poly (lactic-co-glycolic acid) nanoparticles and nanoliposomes for protein delivery in targeted therapy: a comparative in vitro study. *Polymers*. 2020;12:256611. doi:10.3390/polym12112566
21. Kim SR, Ho MJ, Choi YW, et al. Improved drug loading and sustained release of entecavir-loaded PLGA microsphere prepared by spray drying technique. *Bull Korean Chem Soc*. 2019;40(4):306–312. doi:10.1002/bkcs.11682